Archives of Civil and Mechanical Engineering (2024) 24:123
https://doi.org/10.1007/s43452-024-00935-4

ORIGINAL ARTICLE

Influence of grain boundary plane distribution on ionic conductivity in yttria-stabilized zirconia sintered at elevated temperatures

Marek Faryna[1] · **Małgorzata Adamczyk-Habrajska**[2] · **Marta Lubszczyk**[3]

Received: 9 October 2023 / Revised: 23 January 2024 / Accepted: 19 March 2024 / Published online: 16 April 2024
© The Author(s) 2024

Abstract
The paper investigates electrical properties of fully stabilized zirconia, which is widely applied as a solid electrolyte in electrochemical devices such as solid oxide fuel cells. High ionic conductivity of these materials is crucial for effective operating of the devices; however, grain boundary resistivity limits conductivity in polycrystalline ceramics. Thus, optimisation of the microstructure of zirconia is necessary from an application point of view. Based on three-dimensional electron backscatter diffraction (3D EBSD) data, the research employed a complex impedance spectroscopy to establish a correlation between microstructure of cubic zirconia sinters and their conductivity. Samples with different levels of anisotropy in grain boundary plane parameters were investigated. The obtained results indicate that the conduction of ions through the grain boundaries is higher in the sample with the higher representation of the near-(001) grain boundaries. Such a relationship suggests that an over-representation of low-energy grain boundaries in zirconia polycrystals leads to an increase of ionic conductivity.

Keywords Yttria-stabilized zirconia · Grain boundary plane distribution · Ionic conductivity · Impedance spectroscopy

1 Introduction

Stabilized cubic zirconia is often used as a solid electrolyte in electronic devices such as solid oxide fuel cells (SOFCs). An important parameter of solid electrolytes is the ionic conductivity. However, the grain boundaries (GBs) present in polycrystalline ceramics increase the resistivity of the material. The ion transport properties of the GBs are expected to be dependent on their structure and crystallography. Recently, Dillon et al. [1] measured the three-dimensional microstructure of cubic zirconia (YSZ) and determined relative grain boundary energies for different classes of boundaries. When comparing them with experimental data on the resistance of the YSZ bicrystals [2], it was concluded that the conductivity is higher for the low-energy grain boundaries.

Impedance spectroscopy (IS) is a widely utilized method with applications across various fields of research, spanning from fuel cells, batteries, and semiconductor science to corrosion studies, chemical sensing, and biosensing [3]. The strength of impedance spectroscopy, compared to other methods, lies in its ability to investigate electrochemical processes exhibiting diverse time behaviors. In the case of polycrystalline solid electrolytes, IS allows for separate responses arising from bulk and grain boundaries conduction processes. Complex impedance analysis was applied for the first time to investigate a solid electrolyte by Bauerle [4]. Since then, IS studies have been widely conducted on zirconia-based solid electrolytes [5], including yttria-stabilized ZrO_2 [6].

In this work, 8% yttria-stabilized zirconia-textured samples were examined by complex impedance spectroscopy, which allowed to distinguish bulk and grain boundary resistivity. On the other hand, by utilizing three-dimensional electron backscatter diffraction technique in dual-beam scanning microscope (3D EBSD in FIB SEM), it was possible to analyze GB networks based on five characteristic parameters. Three of these parameters specify the lattice misorientation Δg between the two crystals across a grain

✉ Marek Faryna
m.faryna@imim.pl

[1] Polish Academy of Sciences, Institute of Metallurgy and Materials Science, 25 Reymonta St., 30-059 Kraków, Poland

[2] Faculty of Science and Technology, Institute of Materials Engineering, University of Silesia in Katowice, 1a 75 Pułku Piechoty St., 41-500 Chorzów, Poland

[3] Faculty of Materials Science and Ceramics, AGH University of Krakow, 30 Mickiewicza Av., 30-060 Kraków, Poland

boundary. The misorientation space is parameterized into cells (or bins) with a specific discretization (e.g., 10°) using Bunge Euler angles ($\varphi 1$, Φ, $\varphi 2$). The misorientation domain is parameterized by φ1, cos(Φ), and $\varphi 2$ within the range of 0 to $\pi/2$, 0 to 1, and 0 to $\pi/2$, respectively The other two parameters determine the inclination of the grain boundary normal n. The inclination of the boundary normal in the crystal reference frame is parameterized using two angles (i.e., θ and φ) in the spherical coordinate system. The two angles are parameterized by cos (θ) and φ within the range of 0 to 1 and 0 to 2π, respectively. When parameterizing grain boundary space, the cell size should be large enough to contain a considerable number of observations per cell (or per bin) and small enough to represent the textural features at a sufficient resolution [7]. The aim of this research was to find a correlation between the electrical properties and microstructure of the yttria-stabilized cubic zirconia sintered at elevated temperatures. Such a motivation comes from the requirement to improve the performances of solid oxide fuel cells (SOFCs) used as a potential power source for automotive industry.

2 Experimental

A set of three samples manufactured from a cubic polymorphic form of zirconia doped with 8% yttria were prepared by calcination of co-precipitated hydroxides at 500 °C. The powders of specific surface area $S_w = 70.8 \pm 0.2$ m^2/g were prepared as discs ~ 16 mm in diameter and ~ 1.5 mm high. They were uni-axially pressed at 50 MPa in 20 mm steel die (with the possibility of moving both punches) and after that isostatically re-pressed under 200 MPa to assure maximum homogeneous densification. Total shrinkage of the whole manufacturing process (isostatic pressing and sintering) was about 20%. Then the samples were pressureless sintered at the following temperatures of 1500, 1550, and 1600 °C denoted as 1500, 1500 and 1600, respectively. Soaking time was 20 h for each temperature. The reason that these particular sinters were taken into consideration was the fact that the YSZ samples sintered at the above temperatures revealed much stronger anisotropy compared with the YSZ samples sintered at lower temperatures, where anisotropy appeared to be relatively mild. Quantitative evaluation of the anisotropy based on multiples of the random distribution (MRD) was described in detail elsewhere [8, 9], where the values (in MRD) of grain boundary plane distributions at (001) pole for all YSZ sinters were calculated (Fig. 1).

The mean grain size given in microns and its standard deviation (in parentheses) for sintering temperatures 1500, 1550, and 1600 °C was as follows: 4.6 (2.0), 3.6 (1.5), and 7.0 (3.3), respectively.

The 3D EBSD experiments were described thoroughly in several papers. The influence of sintering conditions on anisotropy of grain boundary networks and microstructure topology in yttria-stabilized zirconia was described in Faryna et al. [8], the evaluation of grain boundary plane distribution in yttria-stabilized polycrystalline zirconia based on 3D EBSD analysis was thoroughly investigated in Bobrowski et al. [9], five-dimensional grain boundary distribution for yttria-stabilized zirconia based on experimentally determined macroscopic boundary parameters was discussed in Faryna and Głowinski [10], microstructural characterization of yttria-stabilized zirconia sintered at different temperatures using 3D EBSD, 2D EBSD, and stereological calculations was evaluated in Bobrowski et al. [11], correlation between microstructure and ionic conductivity in cubic zirconia polycrystals was first described in Faryna et al. [12], three-dimensional microstructural characterization of porous cubic zirconia was presented in Bobrowski et al. [13], and grain boundary geometry and pores morphology in dense and porous cubic zirconia polycrystals were investigated in Bobrowski et al. [14]. All these papers include microstructure investigation results and details of experiment. Thus, any information regarding 3D EBSD experiments on the zirconia sinters by use of FIB SEM can be found elsewhere.

In this work, the authors draw their attention on impedance spectroscopy (IS) experiments. The pellets were cut to obtain samples, which allow dielectric and impedance measurements. Silver electrodes were deposited on polished surface of the samples. The dielectric and impedance data were measured using a Hewlett-Packard type 4192 A impedance analyzer, a Hewlett-Packard type 34,401 A millivolt meter, and a Shimaden FP93 temperature controller. Impedance measurements were carried out in the 20 Hz to 2 MHz frequency range and the temperature range of 550

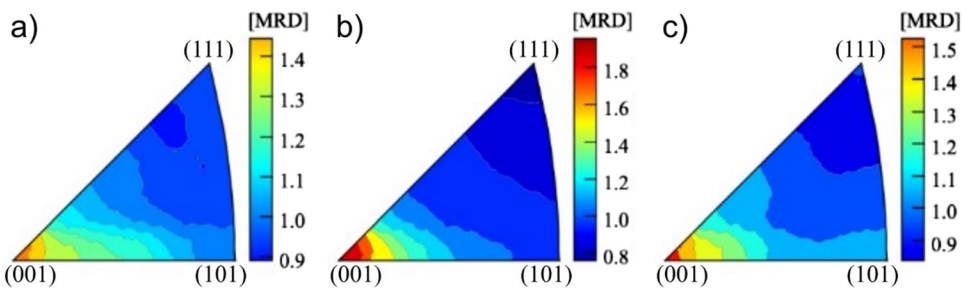

Fig. 1 Populations of boundary planes in the YSZ ceramic sintered at **a** 1500 °C, **b** 1550 °C, and **c** 1600 °C. Distributions were computed for seven data sets separately and for merged data sets corresponding to given sinters. Distribution values (expressed as MRD distributions) are presented in Table 1)

to 650 K in laboratory air. Before the measurements were taken, the samples were rejuvenated. Equivalent circuit fitting to obtained data was performed using ZView software (Scribner Associates, USA).

Grain electrical conductivity (σ_{gi}) and total grain boundary electrical conductivity ($\sigma_{total,gb}$) were calculated based on sample geometry based on the following equations:

$$\sigma_{gi} = \frac{L}{S \cdot R_b} \tag{1}$$

$$\sigma_{total,gb} = \frac{L}{S \cdot R_{gb}} \tag{2}$$

where: R_{gi}—electrical resistance of the grains [Ω], $R_{total,gb}$—total electrical resistance of grain boundaries (gb) [Ω], L—sample thickness [cm], and S—cross-sectional surface area [cm^2].

Equation (2) gives only an apparent value of the conductivity of the grain boundaries. However, it is possible to calculate the 'true' value of the grain boundary conductivity, also known as the specific grain boundary conductivity ($\sigma_{sp,gb}$) using the following formula [15]:

$$\sigma_{sp,gb} = \frac{\delta}{d} \cdot \sigma_{total,gb} \tag{3}$$

where: $\sigma_{total,gb}$ is the total grain boundary conductivity [S/cm], d is the average grain size [nm], δ is the grain boundary thickness [nm]. The grain boundary thickness can be calculated based on the following dependence between the microstructural parameters and the electrical properties of the material [15, 16]:

$$\frac{\delta}{d} = \frac{C_b}{C_{gb}} \cdot \frac{\varepsilon_{gb}}{\varepsilon_{gi}} \tag{4}$$

where: C_b, C_{gb} are the bulk and grain boundary capacitance, ε_b, ε_{gb} are the dielectric permeability of the bulk and grain boundaries. Formula (4) is derived from brick layer model under assumption that bulk conductivity is significantly higher than the grain boundaries conductivity. When assuming that bulk and grain boundaries exhibit nearly identical dielectric permittivity ($\varepsilon_{gb} \approx \varepsilon_{gi}$) Eq. (4) can be simplified to:

$$\delta_{gb} = d \cdot \frac{C_{gi}}{C_{gb}} \tag{5}$$

The effective capacitances C_b and C_{gb} can be calculated with the following Eq. [17]:

$$C_i = (R_i^{1-n_i} A_i)^{\frac{1}{n_i}} \tag{6}$$

where: R_i is bulk or grain boundary resistance, n_i and A_i are the parameters that describe the constant phase element (defined as $Z_{CPE_i} = A_i^{-1}(j\omega)^{-n_i}$), which was used for fitting the electric equivalent circuit.

3 Results

The first approach to analyze the relationship between GB density and components of ionic conductivity was presented in Faryna et al. [12]. However, these results were preliminary and did not show, in a precise way, the effect of observed anisotropy in GB plane parameters caused by manufacturing conditions on the electrical properties of the zirconia sinters. This aforementioned paper showed only that both types of resistance, i.e., bulk and GB resistance decreased with the increase of sintering. In the recent paper [8], GB network based on all five parameters in zirconia sinters was thoroughly investigated. That data were used for computing the grain boundary plane distribution (GBPD) showing populations of grain boundaries as a function of their plane parameters. The values of the GBPD were presented as multiples of the random distribution (MRD). A common observation for all GBPDs was under-representation of near-(111) planes and over-representation of near-(001) planes (compared to random boundaries) in all analyzed YSZ samples. The anisotropy appeared to be stronger if grains were larger. This effect was particularly strong in the case of YSZ ceramic sintered in the temperature range from 1500 to 1600 °C showing its maximum at 1550 °C [8].

This raises the question of whether such anisotropy in GB plane parameters affects the electrical properties of the material. To answer this question, electrochemical impedance spectroscopy measurements were carried out on the three selected samples. The variation of real (Z′) and imaginary (Z″) impedance components with frequency at selected temperatures is presented in Fig. 2. In the low-frequency range, Z′ shows weak frequency dependence and high values for all discussed samples. Such a behavior is connected with high resistivity due to the effectiveness of the resistivity of grain boundaries at this frequency range [18, 19]. With a rise in frequency (> 10^4 Hz), Z′ rapidly decreases, corresponding to an increase in AC conductivity. Similar Z value changes are observed in other materials, e.g., in lead-free $Na_{0.5}Bi_{0.5}TiO_3$ ceramics [20] and vanadium-modified $BaBi_2Nb_2O_9$ ceramics [21]. The measurement points described the Z″(f) relationship forms a curve with a broadened minimum at low-frequency range and diffuse maximum at high frequency. It is worth to notice that the broadening degree of the mentioned minimum is exceptionally high for the sample sintered at 1550 °C. In turn, the maxima visible on the Z″(f) curves are connected with the space charge relaxation. Their location on the frequency axis is strongly dependent on the temperature. Namely, the growth of temperature caused shifts of the mentioned maximum to the higher frequencies. This

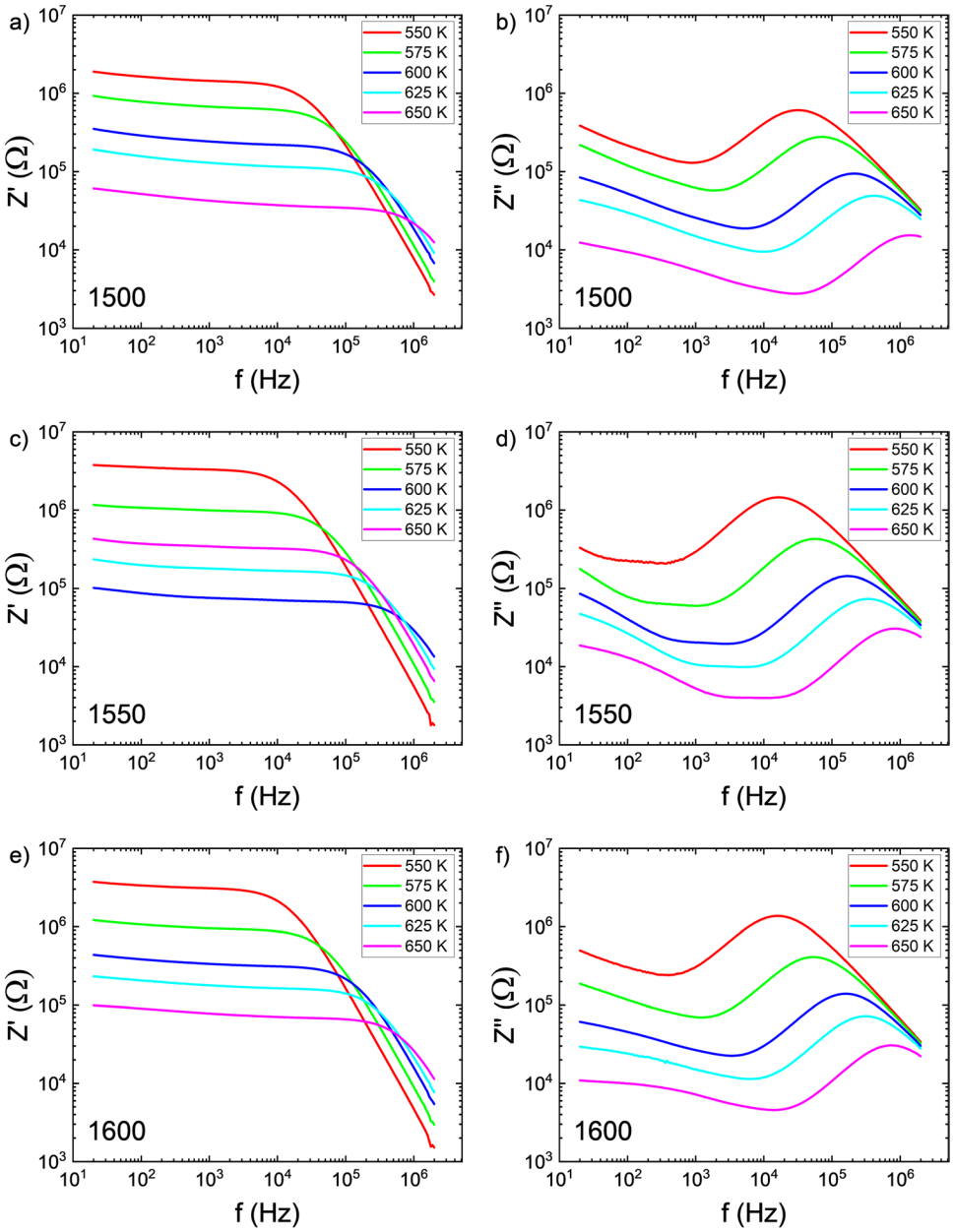

Fig. 2 The frequency dependencies of real (**a**, **c**, **e**) and imaginary (**b**, **d**, **f**) part of the impedance at various temperature for **a**, **b** 1500, **c**, **d** 1550, and **e**, **f** 1600 ZrO_2 sinters

behavior is characteristic for the materials in which the microstructure is characterized by the presence of grains and grain boundaries. In this sense, the role of active areas play grain boundaries, which become a reservoir of space charge. The speed of these charge carriers increases with an increase in temperature, as a result of which the relaxation time of the moving charges is shortened and the frequency f_{max} shifts to higher values [22].

Figure 3 shows Nyquist plots obtained for investigated sinters at temperatures in range of 550 K to 650 K. The characteristics presented have the shape of a deformed semicircle and a fragment of the next one. The deformations indicate that the observed semicircle consists of two overlapping semicircles representing grains and GBs, and the visible fragment of the third semicircle is associated with the response of the near-electrode regions. Therefore, a description of the examined samples can be achieved using an equivalent circuit consisting of 3 Voigt elements, in which capacitance has been replaced with a CPE—constant phase element (insert in Fig. 3). These Voit elements correspond to the interior of the grains, the grain boundaries, and the electrode [4], respectively.

The parameters obtained from the equivalent circuit allowed to determine the electrical conductivity (σ_{gi}) and the electrical conductivity ($\sigma_{total,gb}$) (Eqs. 1 and 2). The average thickness of the grain boundaries (δ) based on formula (Eq. 5) was calculated. All necessary information about the grain size, GBPD at (001) plane, and the calculated GB

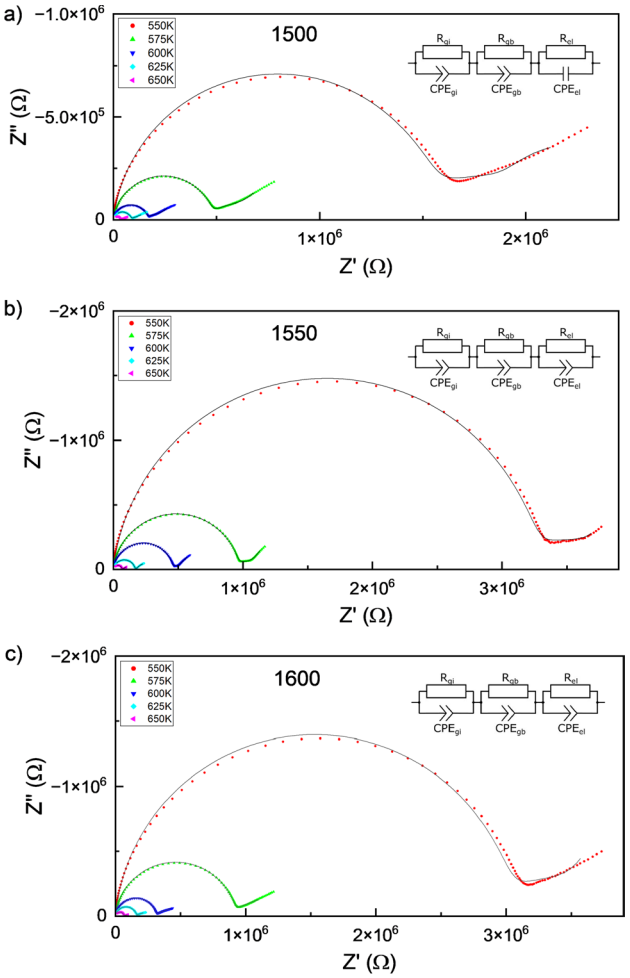

Fig. 3 Impedance spectrums for the **a** 1500, **b** 1550, and **c** 1600 sinters. Points represent experimental data, line represents a fitted curve

thickness are presented in Table 1. It is worth noting that the smallest δ was obtained for the sample sintered at 1500 °C.

The determined GB thicknesses allowed also for the calculation of the specific GB conductivity (Eq. 3). The comparison of the electrical conductivity (σ_{gi}) and specific GB conductivity between the measured samples is presented in Fig. 4 in the form of Arrhenius plots. The linear nature of the presented plots indicates the activating form of conductivity processes. The activation energy of the conductivity of the grain interior ($E_{a(gi)}$) and the grain boundaries ($E_{a(sp,gb)}$) were determined based on the Arrhenius relationship:

$$\sigma = \sigma_0 \exp\left(\frac{-E_a}{kT}\right) \tag{7}$$

where E_a is the activation energy of the conductivity process [eV], k is the Boltzmann constant [eV/K], T is temperature [K], and σ_o is a pre-exponential factor [S K/cm]. The calculated activation energies are listed in Table 1.

The temperature-dependent characteristic of conductivities of the grains (Fig. 4a) has the same slope, which determines the similar value of the activation energy of this process. On the other hand, the plots of GB conductivities vs. temperature are significantly different. Namely, the conductivity and activation energy obtained for the sample sintered at 1550 °C are higher than the ones sintered at 1500 and 1600 °C sintering temperatures.

4 Conclusion

The use of complex impedance spectroscopy confirmed the existence of non-Debye type of relaxation process in the materials, which is connected with the grain and grain boundary effects. An equivalent circuit has been proposed based on the brick layer model for the observed electrical response of the sample. The grain interior and grain boundary conductivity were calculated based on the equivalent circuit. Both values increase with the rise in temperature for all the samples. Moreover, the obtained conductivity values show that the ion conduction process through the GBs is more favorable in the case of the sample denoted as 1550, which shows relatively strong anisotropy with the highest value MRD for GBPD (Table 1). This fact can be explained as follows: low-energy (001) GBs have higher transverse ionic conductivity. Hence, a sample with an over-representation of such a kind of GBs has greater ion conductivity than samples with more random microstructures. The results obtained correlate well with the hypothesis presented in [1].

Table 1 Microstructural and electrical characteristics of investigated sinters

Sample	GBPD at (001) [MRD]	Mean grain size [μm]	GB thickness (δ) [nm]	$E_{a(gi)}$ [eV]	$E_{a(sp,gb)}$ [eV]
1500	1.44 ± 0.04	4.6 ± 2.0	3.16	1.12 ± 0.004	0.73 ± 0.04
1550	1.95 ± 0.05	3.6 ± 1.5	2.31	1.13 ± 0.003	1.51 ± 0.03
1600	1.58 ± 0.07	7.0 ± 3.3	4.13	1.12 ± 0.003	0.80 ± 0.03

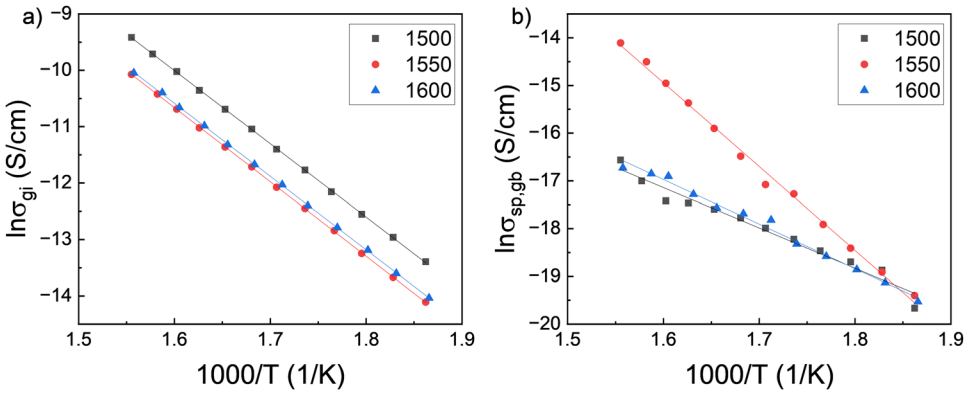

Fig. 4 Temperature dependence of **a** grain interior conductivity and **b** specific grain boundary conductivity in the form of Arrhenius plots for investigated sinters

Acknowledgements The results in this publication were obtained as a part of research financed by the National Science Centre under contract DEC-2017/27/B/ST8/00143—"Project: Grain boundary orientation distribution related to ionic conductivity in zirconia ceramics".

Author contributions MF: 3D EBSD experiments, reviewing and editing. MAH: running impedance spectroscopy experiments. ML: original draft and performing calculations.

Funding This study was supported by Narodowe Centrum Nauki, 2017/27/B/ST8/00143, Marek Faryna.

Data availability Data available on request from the authors.

Declarations

Conflict of interest The authors declare that they have no known competing financial interests or personal relationships that could have appeared to influence the work reported in this paper.

Ethical approval This article does not contain any studies with human participants or animals performed by any of the authors.

Open Access This article is licensed under a Creative Commons Attribution 4.0 International License, which permits use, sharing, adaptation, distribution and reproduction in any medium or format, as long as you give appropriate credit to the original author(s) and the source, provide a link to the Creative Commons licence, and indicate if changes were made. The images or other third party material in this article are included in the article's Creative Commons licence, unless indicated otherwise in a credit line to the material. If material is not included in the article's Creative Commons licence and your intended use is not permitted by statutory regulation or exceeds the permitted use, you will need to obtain permission directly from the copyright holder. To view a copy of this licence, visit http://creativecommons.org/licenses/by/4.0/.

References

1. Dillon SJ, Shen YF, Rohrer GS. Grain boundary energies in yttria-stabilized zirconia. J Am Ceram Soc. 2022;105:2925–31. https://doi.org/10.1111/jace.18283.
2. Ye F, Yin CY, Ou DR, Mori T. Relationship between lattice mismatch and ionic conduction of grain boundary in YSZ. Prog Nat Sci Mater Int. 2014;24:83–6. https://doi.org/10.1016/j.pnsc.2014.01.007.
3. Lazanas AC, Prodromidis MI. Electrochemical Impedance Spectroscopy— A Tutorial. ACS Meas Sci Au. 2023;3(3):162–93. https://doi.org/10.1021/acsmeasuresciau.2c00070.
4. Bauerle JE. Study of solid electrolyte polarization by a complex admittance method. J Phys Chem Solids. 1969;30(12):2657–70. https://doi.org/10.1016/0022-3697(69)90039-0.
5. Liu T, Zhang X, Wang X, Yu J, Li L. A review of zirconia-based solid electrolytes. Ionics. 2016;22:2249–62. https://doi.org/10.1007/s11581-016-1880-1.
6. Zakaria Z, Abu Hassan SH, Shaari N, Yahaya AZ, Boon Kar Y. A review on recent status and challenges of yttria stabilized zirconia modification to lowering the temperature of solid oxide fuel cells operation. Int J Energy Res. 2020;44(2):631–50. https://doi.org/10.1002/er.4944.
7. Saylor DM, Morawiec A, Rohrer GS. Distribution of grain boundaries in magnesia as a function of five macroscopic parameters. Acta Mater. 2003;51:3663–74.
8. Faryna M, Głowiński K, Chulist R, Pędzich Z. Influence of sintering conditions on anisotropy of grain boundary networks and microstructure topology in yttria-stabilized zirconia. Metall Mater Trans A. 2023. https://doi.org/10.1007/s11661-023-07171-0.P.
9. Bobrowski P, Faryna M, Głowiński K. Evaluation of grain boundary plane distribution in yttria stabilized polycrystalline zirconia based on 3D EBSD analysis. Mater Charact. 2016;122:137–41.
10. Faryna M, Głowinski K. Five dimensional grain boundary distribution for yttria stabilized zirconia based on experimentally determined macroscopic boundary parameters. Acta Mater. 2022;226:117606–17.
11. Bobrowski P, Faryna M, Pędzich Z. Microstructural characterization of yttria-stabilized zirconia sintered at different temperatures using 3D EBSD, 2D EBSD and stereological calculations. J Mater Eng Perform. 2017;26:4681–7.
12. Faryna M, Bobrowski P, Pędzich Z, Bućko MM. Correlation between microstructure and ionic conductivity in cubic zirconia polycrystals. Mater Lett. 2015;161:352–4.
13. Bobrowski P, Pędzich Z, Faryna M. Three-dimensional microstructural characterization of porous cubic zirconia. Micron. 2015;78:73–8.
14. Bobrowski P, Faryna M, Pędzich Z. Investigation of grain boundary geometry and pores morphology in dense and porous cubic zirconia polycrystals. Mater Res Bull. 2014;57:203–9.
15. van Dijk T, Burggraaf AJ. Grain boundary effects on ionic conductivity in ceramic GdxZr1–xO2–(x/2) solid solutions. Phys Status Solidi. 1981;63:229–40. https://doi.org/10.1002/pssa.2210630131.

16. Guo X, Waser R. Electrical properties of the grain boundaries of oxygen ion conductors: acceptor-doped zirconia and ceria. Prog Mater Sci. 2006;51:151–210. https://doi.org/10.1016/j.pmatsci.2005.07.001.
17. Hirschorn B, Orazem ME, Tribollet B, Vivier V, Frateur I, Musiani M. Determination of effective capacitance and film thickness from constant-phase-element parameters. Electrochim Acta. 2010;55:6218–27. https://doi.org/10.1016/j.electacta.2009.10.065.
18. Arshad M, Ahmed AS, Azam A, Naqvi AH. Exploring the dielectric behaviour of Co doped ZnO nanoparticles synthesized by wet chemical route using impedance spectroscopy. J Alloys Compd. 2013;577:469–74. https://doi.org/10.1016/j.jallcom.2013.06.035.
19. Ansari SA, Nisar A, Fatma B, Khan W, Naqvi AH. Investigation on structural, optical and dielectric properties of Co doped ZnO nanoparticles synthesized by gel-combustion route. Mater Sci Eng B. 2012;177:428–35. https://doi.org/10.1016/j.mseb.2012.01.022.
20. Suchanicz J, Kluczewska-Chmielarz K, Sitko D, Jagło G. Electrical transport in lead-free Na0.5Bi0.5TiO$_3$ ceramics. J Adv Ceram. 2021;10:152–65. https://doi.org/10.1007/s40145-020-0430-5.
21. Adamczyk M, Kozielski L, Bochenek D, Radoszewska D, Pawełczyk M, Wodecka-Duś B. Impedance spectroscopy of vanadium modified BaBi2Nb2O9 ceramics. Eur Phys J B. 2016;89:1–5. https://doi.org/10.1140/epjb/e2016-60407-2.
22. Dutta S, Choudhary RNP, Sinha PK. Impedance spectroscopy studies on Fe3+ ion modified PLZT ceramics. Ceram Int. 2007;33(1):13–20. https://doi.org/10.1016/j.ceramint.2005.07.010.

Publisher's Note Springer Nature remains neutral with regard to jurisdictional claims in published maps and institutional affiliations.